WITHDRAWN: Asymmetrical response of summer rainfall in East Asia to CO_2 forcing

Se-Yong Song
Hanyang University
Sang-Wook Yeh
swyeh@hanyang.ac.kr

Hanyang University
Soon-Il An
Yonsei University https://orcid.org/0000-0002-0003-429X
Jong-Seong Kug
Pohang University of Science and Technology
Seung-Ki Min
Pohang University of Science and Technology https://orcid.org/0000-0002-6749-010X
Seok-Woo Son
Seoul National University
Jongsoo Shin
Yonsei University

Article

Keywords: hydrology, CO2 concentration

Posted Date: January 19th, 2021

DOI: https://doi.org/10.21203/rs.3.rs-146325/v1

Additional Declarations: There is **NO** Competing Interest.

Version of Record: A version of this preprint was published at Science Bulletin on August 1st, 2021. See the published version at https://doi.org/10.1016/j.scib.2021.08.013.

EDITORIAL NOTE:

The full text of this preprint has been withdrawn by the authors while they make corrections to the work. Therefore, the authors do not wish this work to be cited as a reference. Questions should be directed to the corresponding author.

Abstract

Understanding the regional hydrological response to varying CO2 concentration is critical for cost-benefit analysis of mitigation and adaptation polices in the near future. To characterize summer monsoon rainfall change in East Asia due to a change in the CO2 pathway, we used the Community Earth System Model (CESM) with 28 ensemble members in which the CO2 concentration increases at a rate of 1% per year until its quadrupling peak, i.e., 1,468 ppm (ramp-up period), followed by a decrease of 1% per year until the present-day climate conditions, i.e., 367 ppm (ramp-down period). Although the CO2 concentration change is symmetric in time, the rainfall response is not symmetric. The amount of summer rainfall in East Asia is much larger during a ramp-down period than during a ramp-up period when the two periods of the same CO2 concentration are compared. This asymmetrical rainfall response is mainly due to an enhanced El Niño-like warming pattern as well as an increase in the meridional sea surface temperature gradient in the western North Pacific during a ramp-down period. These sea surface temperature patterns enhance the atmospheric teleconnections to East Asia and the local meridional circulations around East Asia, resulting in more rainfall over East Asia during the ramp-down period. This result implies that the removal of CO2 does not guarantee the return of regional rainfall to the previous climate state with the same CO2 concentration.

Introduction

Continued anthropogenic greenhouse gas emissions pose a threat that could change the climate system. The rapid increase in CO_2 concentration has perturbed radiative forcing in the atmosphere, resulting in an increase in the global mean surface temperature (GMST) of approximately 1°C compared to the pre-industrial period[1, 2]. These changes may also lead to a change in the climate system to a severe, pervasive, and irreversible state, causing devastating changes to the biogeochemical and hydrological cycles, ecosystems, and biodiversity[3, 4]. To reduce such risks, the removal of CO_2 from the atmosphere is considered to be important for achieving climate change mitigation goals[5, 6]. In light of these challenges, understanding the changes to the climate system in response to a carbon dioxide removal (CDR) scenario is critical for climate mitigation and adaption actions in the near future[7].

The climate system response in a CDR scenario is often characterized by hysteresis effects and irreversible changes[7-10]. Recently, the CDR-induced climate change has been investigated using *state-of-the-art climate models[9-13]. Among these, the response of the global hydrological cycle has been widely examined due to the fact that it significantly influences the properties of extreme weather and climate events including droughts, floods, and effects on water supplies. For instance,* the intensified El Ni*ño-like warming pattern induced by a CDR could lead to an asymmetrical response of the rainfall pattern across the globe*[12-14]. In addition, the South Asian monsoon season has also shown an asymmetrical rainfall response to changes in the CO_2 pathway, which has primarily originated from the slow ocean response[12]. These results indicate the need for a wide understanding of the regional rainfall change to the CDR scenario.

The East Asian Summer Monsoon (EASM) is one of the most distinct components of the Asian monsoon system[15]. Its variability has significant impacts on weather and climate conditions with substantial social and economic influence on the local and global community[16-18]. Thus, understanding its future changes is of fundamental societal and scientific importance. The possible changes in the EASM in a warmer climate have been broadly examined using the Coupled Model Intercomparison Projection Phase 5 (CMIP5) climate models[19-21]. It is particularly reported that the EASM rainfall has been projected to increase by 6.4%/K marked by an increase in summer monsoon rainfall[19]. However, there have been fewer studies focusing on the EASM's response to the CDR scenario.

The purpose of this paper is to investigate the rainfall changes in the EASM in response to a change in the CO_2 pathway based on idealized CO_2 experiments (Methods section) and their related physical mechanisms. The results may be helpful for providing useful information on water mitigation and adaptation in this region in a changing climate.

Results

Global mean surface temperature and rainfall response We first show the time series of GMST and rainfall with a change in the CO_2 pathway (Fig. 1b). The GMST continues to increase for several years after a quadrupling peak of CO_2. This phenomenon could be interpreted as a period when the GMST initially responds quickly to a decrease in the CO_2 concentration as the mixed ocean layers cool, followed by a slow decline period due to the release of heat previously accumulated in the ocean[10, 12]. This trend is also seen in the global mean rainfall that continues to increase for almost two decades after the CO_2 quadrupling peak, which is likely due to the increase in the moisture convergence and surface evaporation under global warming conditions as shown in previous studies[19, 22, 23]. Such global rainfall hysteresis could be explained by accumulated heat storage in the ocean[9] and the fast rainfall response to direct CO_2 forcing[24].

During the CO_2 stabilization period, the GMST and rainfall remains higher than the PD climate state when the CO_2 concentration is the same (Figs. 1a,b). The equilibrium state can be reached when CO_2 stabilization forcing is used for more than 1,000 years[25]. These results further emphasized the ocean's large thermal inertia[9, 25], implying that the response of the GMST and rainfall in a changing CO_2 pathway are conditionally irreversible.

Asymmetrical summer rainfall response in East Asia to a change in the CO_2 pathway *Hereafter, we analyze the regional rainfall pattern over East Asia between the ramp-up period (2090-2139, herein referred to as the RU period) and ramp-down period (2141-2190, hereafter referred to as the RD period) during boreal summer (June-July-August) (Fig. 2a and see also Fig. 1a).* It should be noted that we select two periods when the CO_2 concentration is the same in both the RU period and RD period. Despite having the same CO_2 concentration in the RU and RD periods, we find that the amount of rainfall significantly

increases in the EASM region from the RU period to the RD period (Fig. 2a). In contrast, it decreases in the western North Pacific, which will be discussed later.

Figure 2b displays the time series of the average rainfall amount in East Asia (28 -42 N, 105 -150 E, box in Fig. 2a) during summer from the ramp-up period to the stabilization period. Similar to the changes in the global mean rainfall (Fig. 1b), EASM rainfall also continues to increase for almost two decades after the CO_2 quadrupling peak. The climatological amount of rainfall in the PD simulation is 5.54 mm per day during summer; therefore, it increases by almost 20% during the quadrupling peak of the CO_2 concentration. Then, it gradually decreases until the stabilization period. In addition, the decreasing rate of EASM rainfall during the ramp-down period is smaller than its increasing rate during the ramp-up period. This results in the enhancement of summer rainfall in East Asia despite the same CO_2 concentration in the RU and RD periods (Fig. 2a).

The tropical Pacific SST response to the change in the CO_2 pathway To understand these asymmetric changes in the EASM rainfall, it is essential to examine the response of SST during summer with a change in the CO_2 pathway. In particular, the changes in the tropical SST in response to CO_2 forcing could account for a large portion of the regional rainfall pattern via atmospheric teleconnection as well as the response of the tropical rainfall pattern[13, 14, 26-28]. It is found that the tropical Pacific SST response is characterized by an El Ni*ño-like warming pattern during both the RU and RD periods (Figs. 3a,b). Note that the SST pattern is obtained from the* deviation in the ensemble mean climatological SST from a PD simulation (Methods). Furthermore, *an El Niño-like SST warming pattern is strengthened during the RD period, resulting in an asymmetrical response of the SST in the tropical Pacific* between the RU period and the RD period despite having the same CO_2 concentrations *(Fig. 3c), which is* consistent with the results of previous studies based on ramp-up and ramp-down CO_2 experiments using different climate models[13, 14, 29]. These researchers inferred that both a reduction in ocean stratification and a continuous weakening of the Walker circulation since the peak of the CO_2 concentration would serve to produce an enhanced El Ni*ño*-like warming pattern during the RD period. They further speculated that the ocean changes are the driving mechanism that then feed back into the changes in the Walker circulation. However, it is still necessary to understand the detailed processes leading to an enhanced El Ni*ño*-like warming during the RD period when a different climate model is used.

Figure 4a displays the strength of the Walker circulation defined as the sea level pressure difference between the central to eastern Pacific (5 S-5 N, 200 -280 E) and the Indian Ocean/western Pacific (5 S-5 N, 80 -160 E)[30]. The magnitude of the Walker circulation in a changing CO_2 pathway exhibits an asymmetrical response (Fig. 4a). While the intensity of the Walker circulation gradually weakens until the quadrupling peak of the CO_2 concentration, its intensity slowly recovers during the entire period of ramp-down and it continues to recover until the end of the stabilization period. The slow recovery of the Walker circulation intensity during the RD period is associated with an enhanced El Ni*ño*-like SST warming pattern via atmosphere-ocean coupled processes[31] compared to that during the RU period.

To explain this phenomenon, we emphasize the reduced ocean thermal stratification in the central-to-eastern tropical Pacific where the climatological mean upwelling is the most dominant (figure not shown) during the RD period. The reduced ocean thermal stratification induces warming through the *vertical advection of warm subsurface water by the climatological-mean upwelling in the central-to-eastern tropical Pacific. This results in an enhanced El Niño-like SST response as well as its associated slow recovery of Walker circulation via atmosphere-ocean coupled processes during the RD period. To examine this, we show the time series of* ocean thermal stratification, which is defined as the difference between the mixed-layer (30-100m) and sub-thermocline layer (150-230m) ocean temperature *in the central-to-*eastern tropical Pacific (5 S-5 N, 190 -250 E) (Fig. 4b). During the ramp-up period, both the mixed-layer and sub-thermocline layer ocean temperatures tend to warm; however, the mixed-layer temperature warms faster than that in the sub-thermocline layer. This results in a strengthening of the ocean thermal stratification during the RU period. Meanwhile, after the CO_2 quadrupling peak, the mixed-layer temperature starts to cool, while the lower ocean temperature continues to warm, leading to a rapid decline in ocean stratification. Therefore, the continuous ocean warming in the sub-thermocline layer after the CO_2 quadrupling peak leads to an asymmetrical response of ocean stratification from the RU period to the RD period. This process contributes to an enhanced El Ni*ño*-like SST warming as well as its associated slow recovery of Walker circulation during the RD period.

In addition to the mechanism noted above, we suggest that the equatorward migration of the Intertropical Convergence Zone (ITCZ) leads to an enhanced El Niño-like SST warming pattern during the RD period. There is asymmetrical hemispheric warming in the Southern Hemisphere relative to the Northern Hemisphere from the RU period to the RD period (Supplementary Fig. 1), which originates from the large heat capacity of the Southern Ocean. This inter-hemispheric asymmetrical warming pattern may cause an equatorward shift of ITCZ during the RD period compared to that during the RU period, because the ITCZ tends to migrate toward the warmer hemisphere[32, 33] *(Fig. 5)*. Figure 5a clearly shows that the latitudinal position of ITCZ shifted more equatorward after the quadrupling peak of the CO_2 concentration, which is consistent with the changes in rainfall in the tropical Pacific basin between the RU period and the RD period (Figs. 5b,c). An equatorward shift of ITCZ causes a weakening of the trade winds and thus acts to favor an El Ni*ño*-like warming *via reducing evaporative cooling and upwelling[33-35], resulting in enhanced El Niño-like warming during the RD period.*

Atmospheric circulation response and its impacts on rainfall in East Asia *We argue that the asymmetrical response of rainfall in East Asia between the RU and the RD period (see Fig. 2a) is partly due to the enhanced* El Ni*ño-like SST pattern (Fig. 3c) through atmospheric teleconnection[28, 36-38]. To support this notion, we analyze the large-scale zonal and meridional overturning atmospheric circulation pattern.*

There is an asymmetrical response of the zonal overturning atmospheric circulation averaged for 20 S-20 N between the RU and the RD period (Fig. 6a). There are distinct strong upward and *downward motions in the eastern tropical Pacific and the western tropical Pacific, respectively, which is consistent with a weakening of Walker circulation during the RD period. This result indicates that the anomalous downward*

motion over the western North Pacific region contributes to the more suppressed rainfall anomalies over the western North Pacific region during the RD period compared with those during the RU period (see also Fig. 2a). Furthermore, these large-scale atmospheric vertical motions in the western tropical Pacific are responsible for the meridional overturning atmospheric circulation to East Asia[39, 40]*. Figure 6b displays the cross-sections of the differences in the zonally (110-145°E) averaged overturning circulation patterns from the tropics to East Asia* between the RU and RD periods. The downward motions and low-level divergences over the western tropical Pacific led to strong updrafts and northward water vapor transports over 25 *-35 N where the EASM rainfall is significantly enhanced during the RD period compared to that during the RU period. In other words, the large-scale atmospheric overturning circulation pattern, which is related to the enhanced* El Ni*ño-like SST pattern, primarily contributes to the enhanced (suppressed) rainfall anomalies over the EASM (western North Pacific) region between the RU and RD periods.*

On the other hand, the meridional thermal gradients may also contribute to the asymmetrical response of summer rainfall in East Asia through the modulation of monsoon circulation[41-43]*. It should be noted that the SST is warmer in the western North Pacific (*15 -25 N, 120 -150 E*) during the RD period than that during the RU period (see Fig. 3c). This SST warming pattern is induced by the downward motion related to the strengthening of the western North Pacific subtropical high (Fig. 7a and see also Fig. 6b), which is due to the intensified* El Ni*ño-like warming pattern as mentioned above. Concurrently, atmospheric warming with a barotropic structure is prominent over the subtropical Pacific (Fig. 7b). This distinct warming leads to an increase in the meridional temperature gradient from the tropics to* East Asia where the climatological baroclinicity is strong. *Thus,* there is strengthened zonal wind anomalies in the upper troposphere where the westerly jet axis is located via the thermal wind balance[44, 45] (Fig. 7c). This acceleration of the jet may promote the convection to its south, forming the rain band in association with the ageostrophic secondary circulation[46, 47]. It leads to anomalous rainfall over East Asia, contributing to increasing EASM rainfall.

We argue that the continued warming in the western North Pacific, which is associated with the *intensified* El Ni*ño-like warming pattern*, contributes to the asymmetrical response of EASM rainfall through the modulation of the atmospheric circulation pattern. It is also noteworthy that the El Ni*ño*-like warming is related to the *enhanced (suppressed) rainfall anomalies over the EASM (western North Pacific) region during summer in the PD simulation (Supplementary Fig. 2), supporting the notion noted above that the enhanced El Niño-like warming causes the asymmetrical response of rainfall in East Asia between the RU and RD periods.*

Discussion

The idealized CO_2 forcing experiments are designed to provide an understanding of the regional hydrological response to direct atmospheric CO_2 removal. We found an asymmetrical response of the East Asian summer monsoon rainfall pattern with a change in the CO_2 pathway. The model results show that the rainfall over the EASM region gradually increased during the RU period. However, it slowly

decreased following the CO_2 decrease during the RD period. This asymmetrical response is mainly due to the intensified El Niño-like warming pattern during the RD period. This SST warming pattern is largely due to the slow warming response of sub-thermocline ocean temperature in the central-to-eastern tropical Pacific, leading to contrasting ocean thermal stratification from the RU period to the RD period. Furthermore, the migration of ITCZ due to the contrast in the asymmetrical hemispheric warming is also associated with the enhanced El Niño-like SST warming pattern during the RD period. Subsequently, anomalous large-scale overturning circulation patterns due to the intensified El Niño-like warming pattern lead to an anomalous upward (downward) motion over EASM (western North Pacific), leading to the enhanced (suppressed) rainfall anomaly. In addition, continued warming over the western North Pacific strengthens the meridional temperature gradient over East Asia where the climatological baroclinicity is strong. This leads to an accelerated westerly jet, which leads to increased rainfall in East Asia by altering the ageostrophic secondary circulation.

It is noteworthy that the EASM rainfall during the CO_2 stabilization period remains higher than that during the PD climate state when the CO_2 concentration is the same (Fig. 2b). This irreversible feature of EASM rainfall may be due to the continued warming over the eastern tropical Pacific and western North Pacific region during the CO_2 stabilization periods (Supplementary Fig. 3), which is associated with the large thermal inertia of the ocean. These results suggest that the asymmetrical response and irreversible change in EASM rainfall are closely linked through oceanic memory.

Methods

CO_2 ramp-up and ramp-down experiments To examine the hydrological response to idealized CO_2 forcing, we use the coupled general circulation model (CGCM) experiments via Community Earth System Model version 1.2.2 (CESM1.2.2)[48]. This CESM1.2.2 configures atmosphere, ocean, sea ice, and land models, and prescribes idealized CO_2 forcing. Each component of CESM1.2.2 is as follows. The atmosphere model is the Community Atmospheric Model on a horizontal resolution of approximately 0.9 $^\circ$ latitude by 1.25° longitude with 30 vertical layers[49]. The Parallel Ocean Program version 2 ocean model had 60 staggered vertical levels with a horizontal resolution of longitudinal 1° and latitudinal 0.5° that decreases to 0.3° latitude near the equator[50]. The land model is the Community Land Model version 4 configured with the carbon-nitrogen cycle[51]. The sea-ice component is the Community Ice Code version 4[52].

We first conduct the present-day climate simulation with a fixed CO_2 concentration (367 ppm) for the simulation period of 900 years. This reference simulation is referred to as a PD simulation. Then, the changing CO_2 pathway with 28 ensemble members is employed. In this study, the atmospheric CO_2 concentration with a 1% increase per year peaks with its quadrupling (i.e., 1,468 ppm) (referred to as the ramp-up period), followed by a decrease of 1% per year until the CO_2 concentration in the present-day climate (referred to as the ramp-down period) as shown in Fig. 1a. The CO_2 stabilization with a

concentration of 367 ppm is continued for 120 years. The 28 ensemble members are identical except for the oceanic initial conditions, which are taken arbitrarily from a PD simulation.

Anomaly calculation We analyze the ensemble mean atmospheric and oceanic variables simulated from the 28 ensemble members to emphasize the role of atmospheric CO_2 forcing by excluding the role of internal variability in the climate system. All of the analyses are based on deviation from the PD climatology from the ensemble mean variables. To test the statistical significance of the difference in the atmospheric and oceanic fields between the ramp-up and -down periods, we use a two-sided Student's *t*-test.

Declarations

Code availability All the NCL and Fortran 90 codes used to generate the results of this study are available from the authors upon request.

References

1. Masson-Delmotte V*, et al. Global Warming of 1.5 OC: An IPCC Special Report on the Impacts of Global Warming of 1.5° C Above Pre-industrial Levels and Related Global Greenhouse Gas Emission Pathways, in the Context of Strengthening the Global Response to the Threat of Climate Change, Sustainable Development, and Efforts to Eradicate Poverty*. World Meteorological Organization Geneva, Switzerland (2018).
2. Morice CP, Kennedy JJ, Rayner NA, Jones PD. Quantifying uncertainties in global and regional temperature change using an ensemble of observational estimates: The HadCRUT4 data set. *Journal of Geophysical Research: Atmospheres* **117**, (2012).
3. Boyd PW. Ranking geo-engineering schemes. *Nature Geoscience* **1**, 722-724 (2008).
4. Keller DP, Feng EY, Oschlies A. Potential climate engineering effectiveness and side effects during a high carbon dioxide-emission scenario. *Nature communications* **5**, 1-11 (2014).
5. Peters GP*, et al.* The challenge to keep global warming below 2 C. *Nature Climate Change* **3**, 4-6 (2013).
6. Vaughan NE, Lenton TM. A review of climate geoengineering proposals. *Climatic change* **109**, 745-790 (2011).
7. Keller DP*, et al.* The carbon dioxide removal model intercomparison project (CDRMIP): rationale and experimental protocol for CMIP6. *Geoscientific Model Development* **11**, 1133-1160 (2018).
8. Mathesius S, Hofmann M, Caldeira K, Schellnhuber HJ. Long-term response of oceans to CO 2 removal from the atmosphere. *Nature Climate Change* **5**, 1107-1113 (2015).
9. Wu P, Wood R, Ridley J, Lowe J. Temporary acceleration of the hydrological cycle in response to a CO2 rampdown. *Geophysical Research Letters* **37**, (2010).

10. Boucher O*, et al.* Reversibility in an Earth System model in response to CO2 concentration changes. *Environmental Research Letters* **7**, 024013 (2012).
11. Armour K, Eisenman I, Blanchard-Wrigglesworth E, McCusker K, Bitz C. The reversibility of sea ice loss in a state-of-the-art climate model. *Geophysical Research Letters* **38**, (2011).
12. Wu P, Ridley J, Pardaens A, Levine R, Lowe J. The reversibility of CO 2 induced climate change. *Climate Dynamics* **45**, 745-754 (2015).
13. Chadwick R, Wu P, Good P, Andrews T. Asymmetries in tropical rainfall and circulation patterns in idealised CO 2 removal experiments. *Climate dynamics* **40**, 295-316 (2013).
14. Ma J*, et al.* Responses of the tropical atmospheric circulation to climate change and connection to the hydrological cycle. *Annual Review of Earth and Planetary Sciences* **46**, 549-580 (2018).
15. Ding Y, Chan JC. The East Asian summer monsoon: an overview. *Meteorology and Atmospheric Physics* **89**, 117-142 (2005).
16. Jiang T, Kundzewicz ZW, Su B. Changes in monthly precipitation and flood hazard in the Yangtze River Basin, China. *International Journal of Climatology: A Journal of the Royal Meteorological Society* **28**, 1471-1481 (2008).
17. Qiu J. Monsoon melee.). American Association for the Advancement of Science (2013).
18. Ha K-J, Lee J-Y, Wang B, Xie S-P, Kitoh A. Asian monsoon climate change-Understanding and prediction.). Korean Meteorological Society (2017).
19. Wang B, Yim S-Y, Lee J-Y, Liu J, Ha K-J. Future change of Asian-Australian monsoon under RCP 4.5 anthropogenic warming scenario. *Climate dynamics* **42**, 83-100 (2014).
20. Seo K-H, Ok J, Son J-H, Cha D-H. Assessing future changes in the East Asian summer monsoon using CMIP5 coupled models. *Journal of climate* **26**, 7662-7675 (2013).
21. Song F, Zhou T, Qian Y. Responses of East Asian summer monsoon to natural and anthropogenic forcings in the 17 latest CMIP5 models. *Geophysical Research Letters* **41**, 596-603 (2014).
22. Hsu Pc, Li T, Luo JJ, Murakami H, Kitoh A, Zhao M. Increase of global monsoon area and precipitation under global warming: A robust signal? *Geophysical Research Letters* **39**, (2012).
23. Lee J-Y, Wang B. Future change of global monsoon in the CMIP5. *Climate Dynamics* **42**, 101-119 (2014).
24. Cao L, Bala G, Caldeira K. Why is there a short-term increase in global precipitation in response to diminished CO2 forcing? *Geophysical research letters* **38**, (2011).
25. Hansen J, Russell G, Lacis A, Fung I, Rind D, Stone P. Climate response times: Dependence on climate sensitivity and ocean mixing. *Science* **229**, 857-859 (1985).
26. Huang P, Xie S-P, Hu K, Huang G, Huang R. Patterns of the seasonal response of tropical rainfall to global warming. *Nature Geoscience* **6**, 357-361 (2013).
27. Xie S-P, Deser C, Vecchi GA, Ma J, Teng H, Wittenberg AT. Global warming pattern formation: Sea surface temperature and rainfall. *Journal of Climate* **23**, 966-986 (2010).

28. Yeh SW*, et al.* ENSO atmospheric teleconnections and their response to greenhouse gas forcing. *Reviews of Geophysics* **56**, 185-206 (2018).
29. Ohba M, Tsutsui J, Nohara D. Statistical parameterization expressing ENSO variability and reversibility in response to CO2 concentration changes. *Journal of climate* **27**, 398-410 (2014).
30. Vecchi GA, Soden BJ, Wittenberg AT, Held IM, Leetmaa A, Harrison MJ. Weakening of tropical Pacific atmospheric circulation due to anthropogenic forcing. *Nature* **441**, 73-76 (2006).
31. Bjerknes J. Atmospheric teleconnections from the equatorial Pacific. *Monthly weather review* **97**, 163-172 (1969).
32. Yoshimori M, Broccoli AJ. Equilibrium response of an atmosphere–mixed layer ocean model to different radiative forcing agents: Global and zonal mean response. *Journal of Climate* **21**, 4399-4423 (2008).
33. Zhou W, Xie S-P, Yang D. Enhanced equatorial warming causes deep-tropical contraction and subtropical monsoon shift. *Nature Climate Change* **9**, 834-839 (2019).
34. Dai A, Wigley T. Global patterns of ENSO-induced precipitation. *Geophysical Research Letters* **27**, 1283-1286 (2000).
35. Schneider T, Bischoff T, Haug GH. Migrations and dynamics of the intertropical convergence zone. *Nature* **513**, 45-53 (2014).
36. Chang C, Zhang Y, Li T. Interannual and interdecadal variations of the East Asian summer monsoon and tropical Pacific SSTs. Part I: Roles of the subtropical ridge. *Journal of Climate* **13**, 4310-4325 (2000).
37. Wang B, Wu R, Fu X. Pacific–East Asian teleconnection: how does ENSO affect East Asian climate? *Journal of Climate* **13**, 1517-1536 (2000).
38. Zhao G*, et al.* A new upper-level circulation index for the East Asian summer monsoon variability. *Journal of Climate* **28**, 9977-9996 (2015).
39. Kosaka Y, Nakamura H. Structure and dynamics of the summertime Pacific–Japan teleconnection pattern. *Quarterly Journal of the Royal Meteorological Society: A journal of the atmospheric sciences, applied meteorology and physical oceanography* **132**, 2009-2030 (2006).
40. Nitta T. Convective activities in the tropical western Pacific and their impact on the Northern Hemisphere summer circulation. *Journal of the Meteorological Society of Japan Ser II* **65**, 373-390 (1987).
41. Zhou T, Zou L. Understanding the predictability of East Asian summer monsoon from the reproduction of land–sea thermal contrast change in AMIP-type simulation. *Journal of Climate* **23**, 6009-6026 (2010).
42. Dai A, Li H, Sun Y, Hong LC, Chou C, Zhou T. The relative roles of upper and lower tropospheric thermal contrasts and tropical influences in driving Asian summer monsoons. *Journal of Geophysical Research: Atmospheres* **118**, 7024-7045 (2013).

43. Webster PJ, Yang S. Monsoon and ENSO: Selectively interactive systems. *Quarterly Journal of the Royal Meteorological Society* **118**, 877-926 (1992).
44. Holton JR. An introduction to dynamic meteorology. *American Journal of Physics* **41**, 752-754 (1973).
45. Zhongda L, Riyu L. Interannual meridional displacement of the East Asian upper-tropospheric jet stream in summer. *Advances in Atmospheric Sciences* **22**, 199 (2005).
46. Horinouchi T. Influence of upper tropospheric disturbances on the synoptic variability of precipitation and moisture transport over summertime East Asia and the northwestern Pacific. *Journal of the Meteorological Society of Japan Ser II* **92**, 519-541 (2014).
47. Chowdary JS, Hu K, Srinivas G, Kosaka Y, Wang L, Rao KK. The Eurasian jet streams as conduits for east Asian monsoon variability. *Current Climate Change Reports* **5**, 233-244 (2019).
48. Hurrell JW*, et al.* The community earth system model: a framework for collaborative research. *Bulletin of the American Meteorological Society* **94**, 1339-1360 (2013).
49. Neale RB*, et al.* Description of the NCAR community atmosphere model (CAM 5.0). *NCAR Tech Note NCAR/TN-486+ STR* **1**, 1-12 (2012).
50. Smith R*, et al.* The parallel ocean program (POP) reference manual: ocean component of the community climate system model (CCSM) and community earth system model (CESM). *LAUR-01853* **141**, 1-140 (2010).
51. Lawrence DM*, et al.* Parameterization improvements and functional and structural advances in version 4 of the Community Land Model. *Journal of Advances in Modeling Earth Systems* **3**, (2011).
52. Hunke EC, Lipscomb WH, Turner AK, Jeffery N, Elliott S. CICE: the Los Alamos Sea Ice Model Documentation and Software User's Manual Version 4.1 LA-CC-06-012. *T-3 Fluid Dynamics Group, Los Alamos National Laboratory* **675**, 500 (2010).

Figures

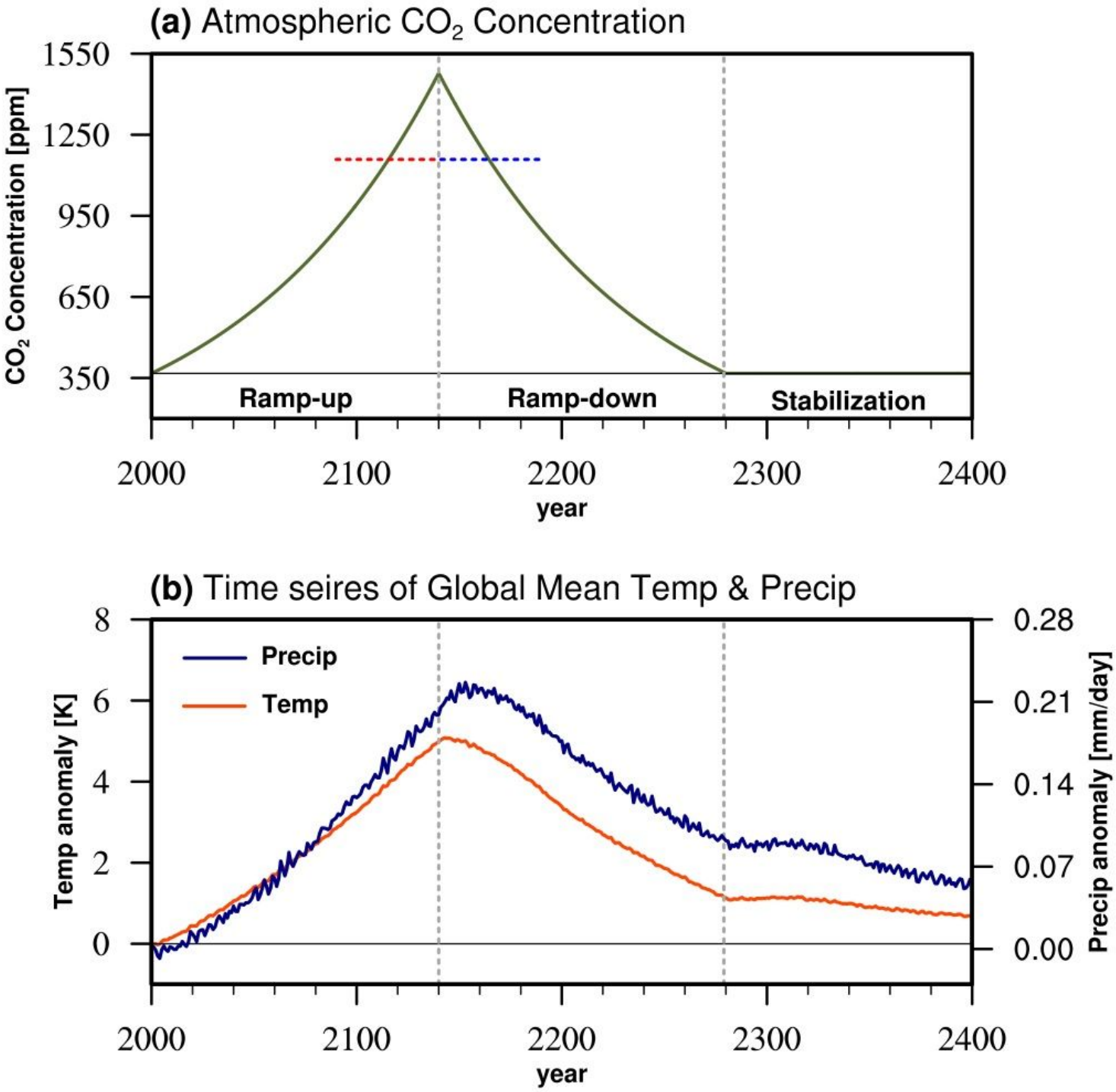

Figure 1

Time series of the (a) CO2 concentration, and (b) annual GMST anomaly (red line, K) and rainfall (blue line). The grey vertical dotted line denotes the CO2 peak and stabilization start year. Red and blue dotted lines as shown in Fig. 1a indicate the two 50-year periods with the same averaged CO2 concentrations (1,159 ppm) in the ramp-up (2090-2139) and ramp-down (2141-2190) periods, respectively.

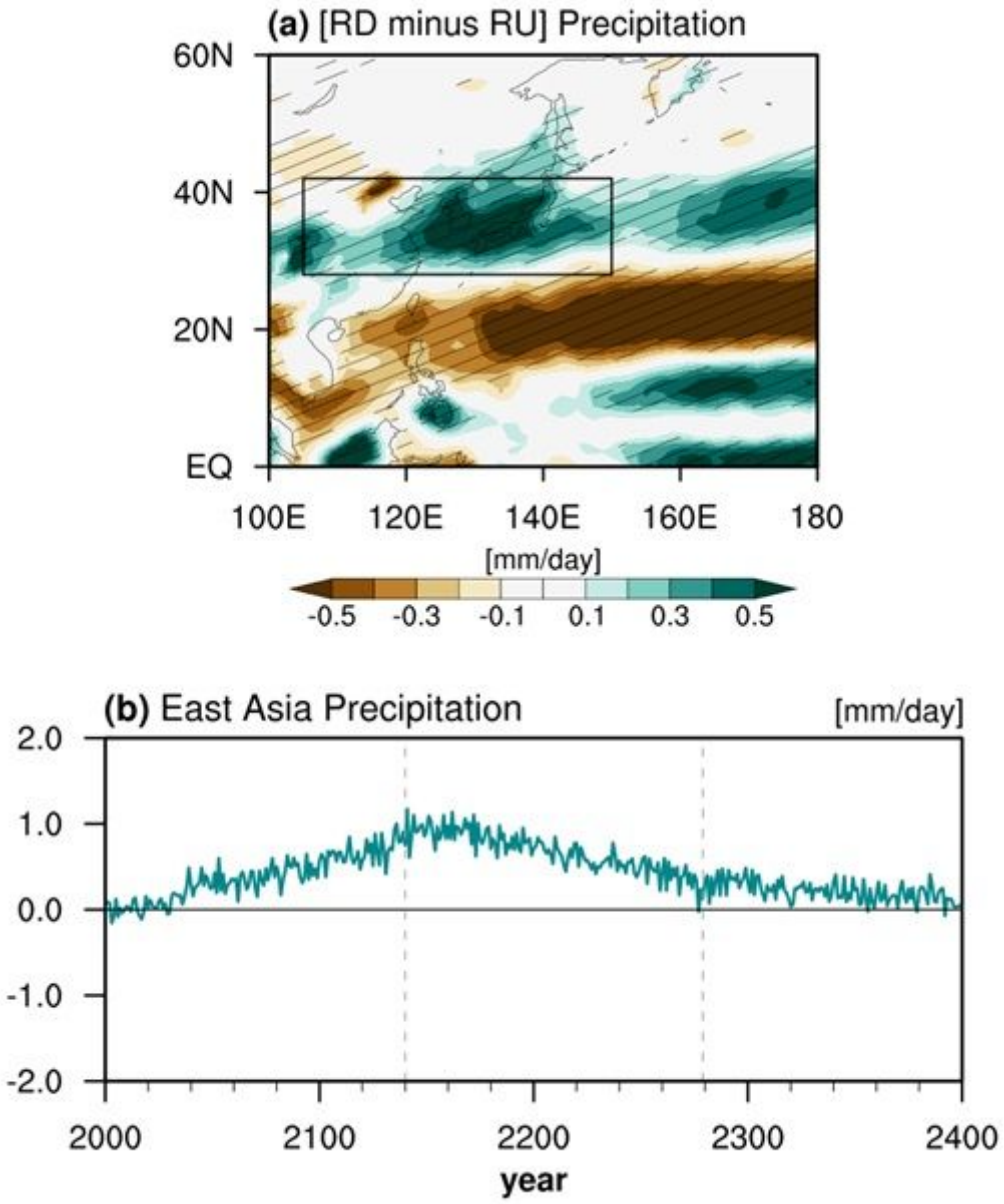

Figure 2

(a) Difference in rainfall anomalies (mm/day) between the ramp-down (2141-2190) and ramp-up (2090-2139) periods during boreal summer. Black hatching denotes that the regions are significant at a 95% confidence level. (b) Time series of summertime rainfall anomalies (mm/day) averaged over the East Asian (Black box in Fig. 2a, 28°-42°N, 105°-150°E) region during boreal summer. Grey vertical dotted line in Fig. 2b denotes CO2 peak and stabilization start year.

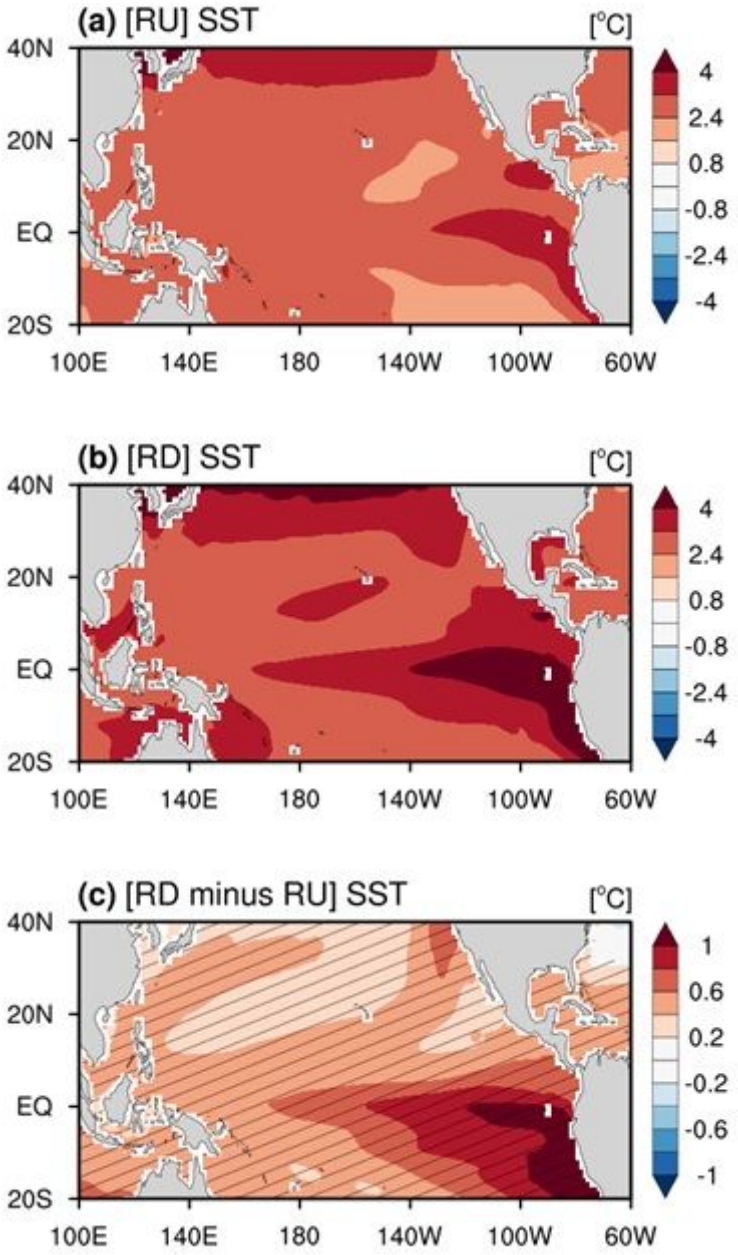

Figure 3

SST anomalies (℃) during (a) the ramp-up (2090-2139) and (b) ramp-down (2141-2190) periods during boreal summer. (c) Difference in SST anomalies (℃) between the ramp-down (2141-2190) and ramp-up (2090-2139) periods during boreal summer. Black hatching denotes that the regions are significant at a 95% confidence level.

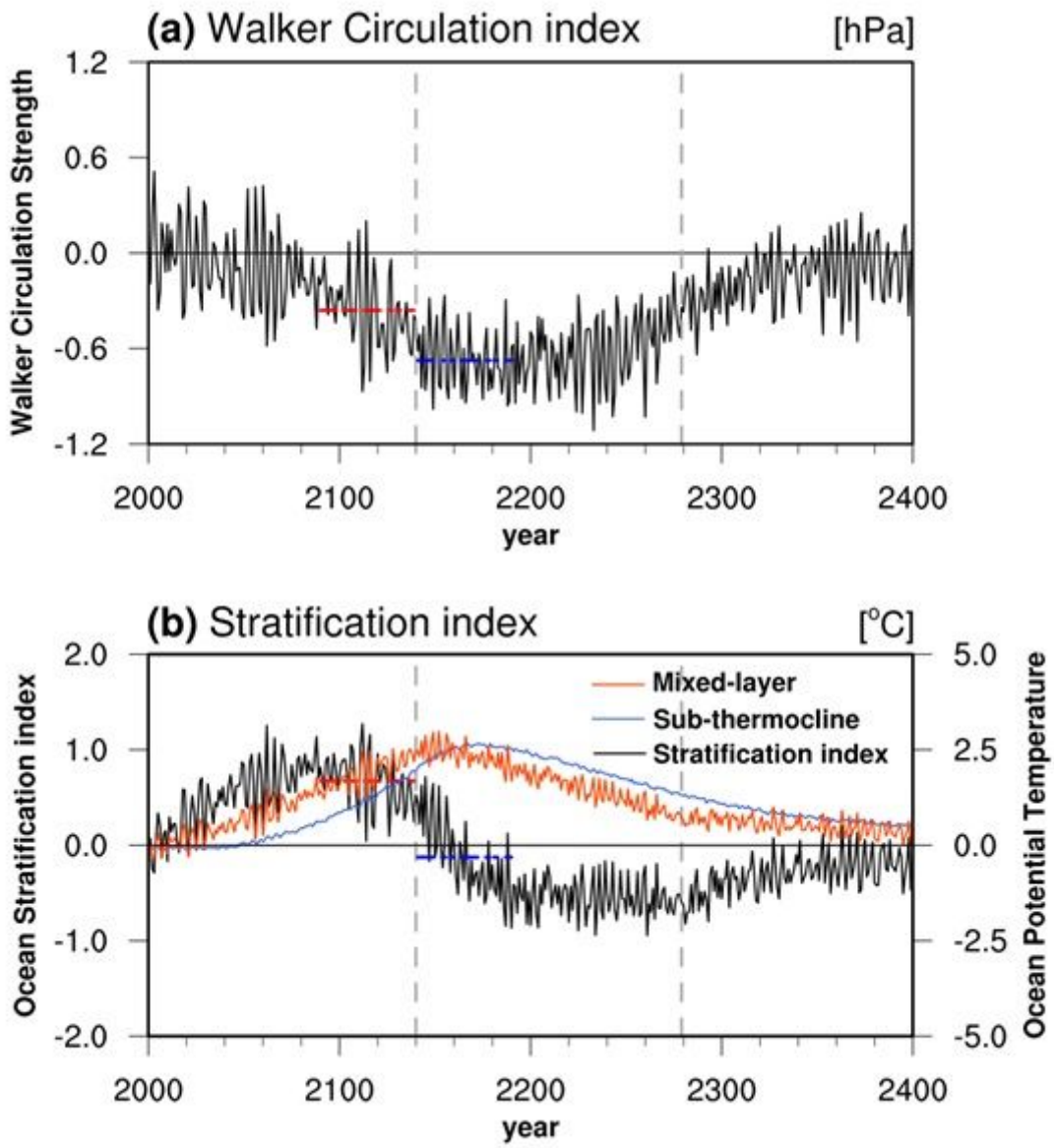

Figure 4

(a) Time series of the Walker circulation index during boreal summer. (b) Time series of the mixed-layer (orange, 30-100m) and sub-thermocline (blue, 150-230m) ocean potential temperature and stratification index (black) in the central-to-eastern tropical Pacific (5°S-5°N, 190°-250°E) during boreal summer. Grey vertical dotted line denotes the CO2 peak and stabilization start year. Red and blue dotted lines indicate the averaged value for each index in the ramp-up (2090-2139) and ramp-down (2141-2190) periods, respectively.

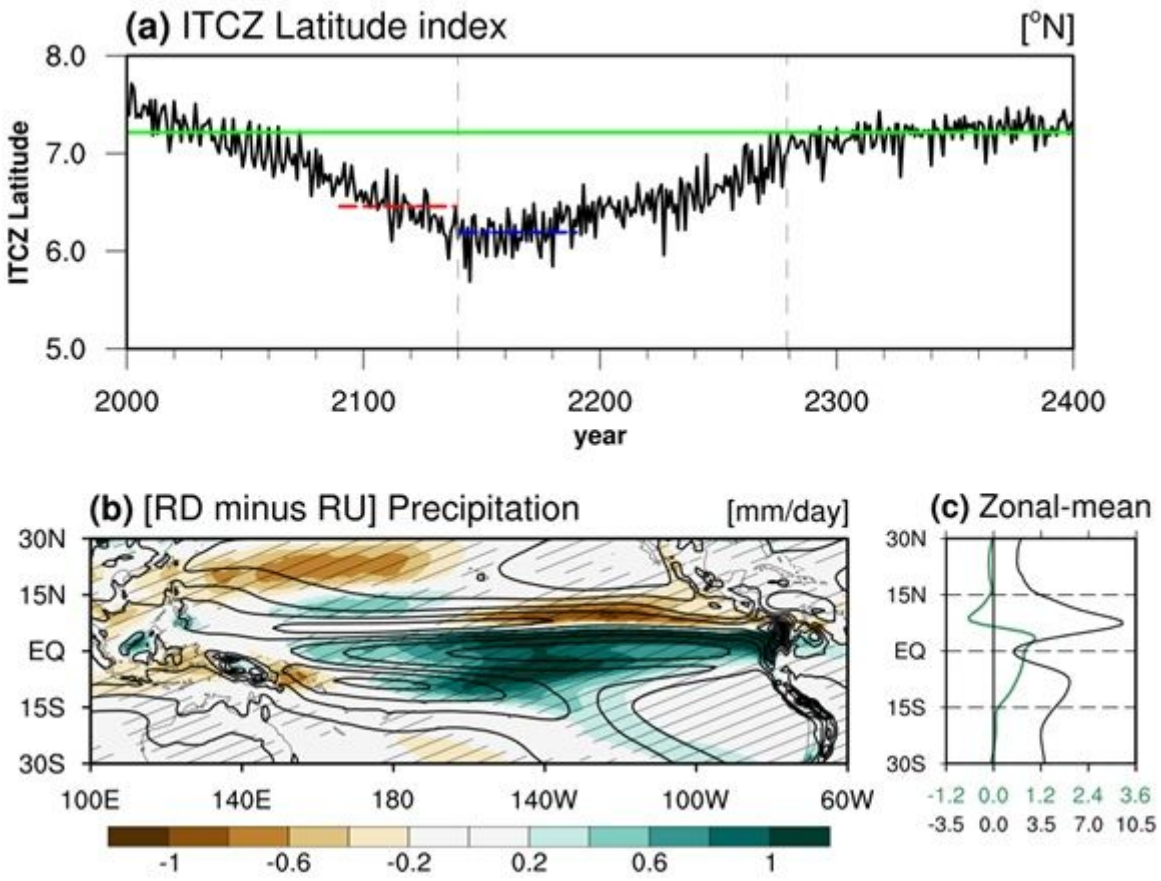

Figure 5

(a) Time series of the ITCZ latitude index. The ITCZ index is obtained from the average value of the latitudes where the rainfall is the strongest at each longitudinal grid (90°W-180°) within 3°S-15°N during boreal summer. Red and blue dotted lines indicate the average value for the ITCZ index in the RU (2090-2139) and RD (2141-2190) periods, respectively. Light green line shows the climatological ITCZ latitude in a PD simulation. (b) Differences in rainfall (shading, mm/day) between the RU period and the RD during boreal summer. Black hatching denotes that the regions are significant at a 95% confidence level. Black contour line indicates the climatological rainfall obtained from the PD simulation. (c) Difference in rainfall averaged for 90°W-180° between the RU period and the RD period during boreal summer (green) with the climatological rainfall averaged for 90°W-180° (black), which was obtained from the PD simulation.

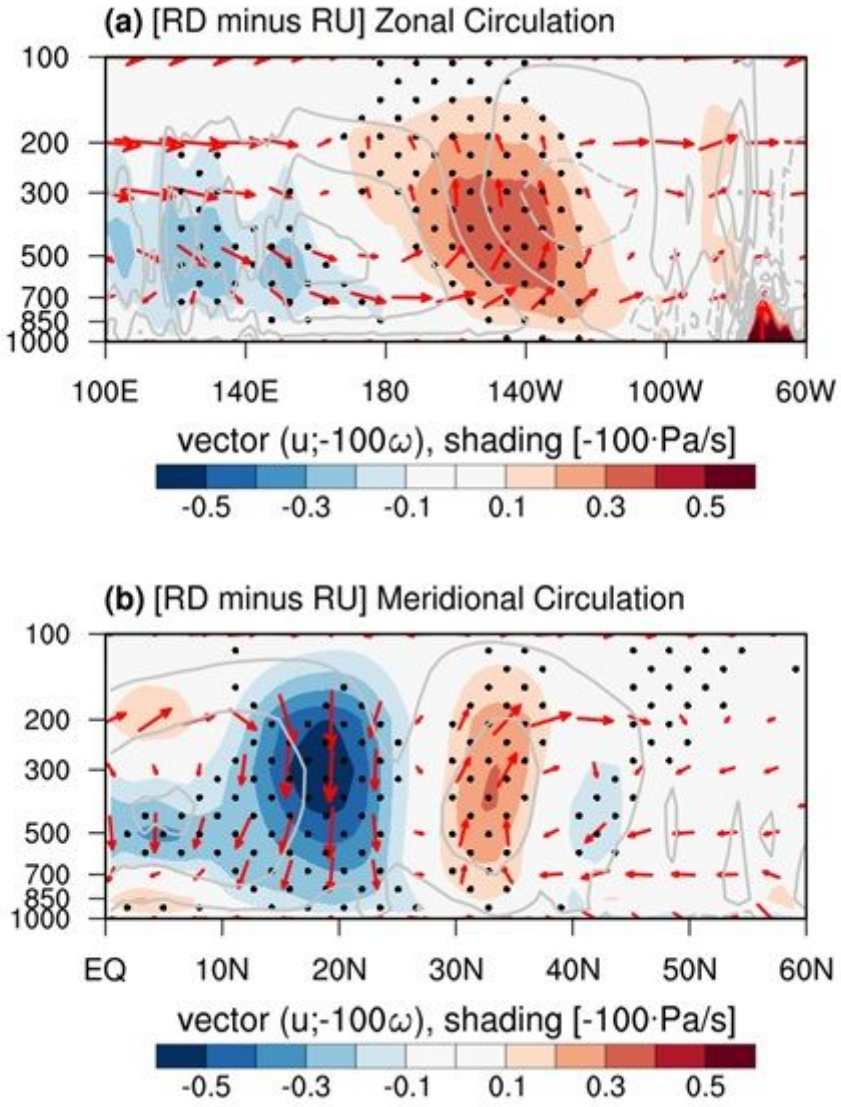

Figure 6

(a) The cross-section of differences in zonal and vertical velocities (red vectors), which are averaged for 20°S-20°N between the ramp-down (2141-2190) and ramp-up (2090-2139) periods during boreal summer. (b) Same as (a), but for meridional and vertical velocities, which are averaged over 110°-145°E. Shaded values are differences in vertical velocities (-102 Pa s-1). Grey contour line indicates the climatological vertical velocities obtained from the PD simulation. Black dots indicate that the regions are significant at a 99% confidence level.

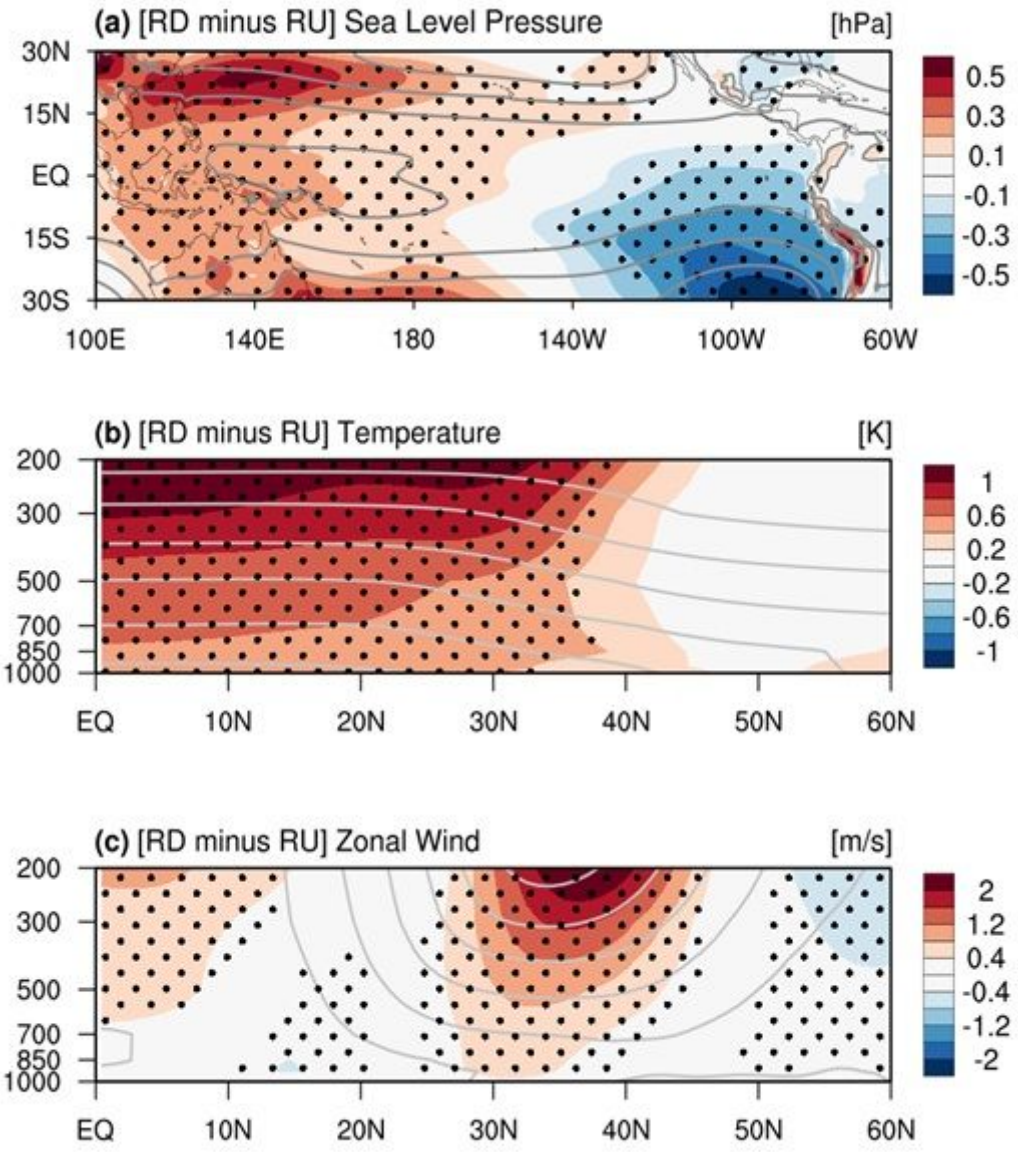

Figure 7

(a) Difference in sea level pressure (SLP) between the ramp-down (2141-2190) and ramp-up (2090-2139) periods during boreal summer. (b) Latitude-height cross-section of the differences in temperature averaged for 105°-150°E between the ramp-down (2141-2190) and ramp-up (2090-2139) periods during boreal summer. (c) is same as (b), but for the zonal wind. Black dots denote that the regions are significant at a 99% confidence level. Grey contour indicates the climatological patterns of each variable obtained from the PD simulation.

Supplementary Files

This is a list of supplementary files associated with this preprint. Click to download.

- AHY2012091NCOMMSI2021.01.08.docx